IDEAL MAGNETOHYDRODYNAMIC STABILITY OF THE SPHEROMAK CONFIGURATION

BY

S.C. JARDIN

JANUARY 19, 1982

PLASMA PHYSICS LABORATORY

PRINCETON UNIVERSITY
PRINCETON, NEW JERSEY

PREPARED FOR THE U.S. DEPARTMENT OF ENERGY,
UNDER CONTRACT DE-AC02-76-CHO-3073.

Ideal Magnetohydrodynamic Stability of the Spheromak Configuration

PPPL--1861

DE82 011310

S. C. Jardin

Plasma Physics Laboratory, Princeton University

Princeton, New Jersey 08544

Abstract

Results are presented of a parametric study of the ideal magnetohydrodynamic stability properties of the spheromak, or compact torus, configuration. In the absence of a nearby conducting wall, the spheromak is always unstable to at least one current driven mode. With a conducting wall at the surface, the spheromak can be unstable to current driven modes if the current is too peaked, i.e., $q_o(R/a) \lesssim 2/3$, or if the shear is too low at the origin. The Mercier criterion sets an upper limit on the pressure gradient everywhere, but configurations that are everywhere Mercier stable can be unstable to pressure driven low-n modes. Stable toroidal configurations exist with a spherical wall separated by half a minor radius, and with $\beta_\theta = 30\%$.

I. INTRODUCTION

The spheromak, or the compact torus, is an axisymmetric closed magnetic field line toroidal plasma confinement configuration with zero vacuum toroidal magnetic field. Toroidal and poloidal currents of comparable magnitude exist in the plasma to generate the poloidal and toroidal confinement magnetic fields. Just as the tokamak is a stellerator with internal toroidal current instead of external helical windings producing the confining poloidal fields, so the spheromak is a tokamak with internal poloidal currents instead of external toroidal field coils producing the confining toroidal fields.

Recent experimental investigations [1-3] have demonstrated that there do exist configurations of the spheromak type that remain stable on the ideal magnetohydrodynamic time scale, that is, over time intervals long compared to the Alfvén wave transit time of the device, $\tau_A = (\mu_o \rho_o)^{1/2} a/B_o$. This is in qualitative agreement with existing theoretical investigations [4-6] which have identified stable configurations with current distributions near the Taylor state in which the current density is everywhere proportional to the magnetic field strength, $\vec{J} = \lambda \vec{B}$. In order to make better quantitative comparisons with experimental results, and to aid in the design of new experiments, it is desirable to have mapped out the theoretical boundaries of the stable operating regimes in the space formed by parameters describing more general current and pressure distributions, different aspect ratios, and a range of plasma cross sectional shapes. Such is the intention of the present paper.

In the next section we discuss the ideal magnetohydrodynamic stability properties of the circular cylindrical spheromak. This is a fictitious configuration in which the torus has been cut and straightened out to become a circular cylinder of radius a, length $2\pi R$, and with periodic boundary

conditions. The usefulness of this model lies in the fact that it has a reduced parameter space and is more amenable to theoretical analysis. We find that a single nine-part diagram adequately summarizes the stability properties of this configuration.

Section III discusses the stability properties of the actual toroidal spheromak. The complexity of toroidal geometry greatly expands the dimension of the parameter space and necesitates the use of large numerical stability codes. However, upon comparing the results we obtain here with those of Section II, we find generally a good correspondence between the stability results for the cylindrical and the toroidal geometry. In exception to this are a small number of new unstable modes which exist in toroidal geometry but have no analoque in the cylindrical spheromak.

II. THE CYLINDRICAL SPHEROMAK

A usefull model for locating and understanding parameter regimes of internal mode stability is provided by considering the periodic cylindrical spheromak. Using standard (r,θ,z) cylindrical coordinates, we define a periodicity length in the z direction of $L \equiv 2\pi/k$, where k is the analog of the reciprocal major radius in a toroidal device, $k \equiv 1/R$. The equilibrium equation in this geometry is

$$\frac{dp}{dr} + \frac{d}{dr}\frac{1}{2}B_z^2 + \frac{B_\theta}{r}\frac{d}{dr}rB_\theta = 0 \quad . \tag{1}$$

The safety factor profile, $q(r) \equiv rkB_z(r)/B_\theta(r)$, is taken to be of the form $q(r) = q_o(1-r^{2\sigma})$, where the plasma boundary is defined by $r = 1$. To parameterize the pressure, we introduce the parameter $0 \leq \alpha \leq 1$ by $dp/dr = -\alpha r B_z^2/8\,(q'/q)^2$. Thus for $\alpha = 0$, the plasma is force free, while

for $\alpha = 1$, the pressure is determined by the condition that it be everywhere marginally stable to ideal interchange modes, according to the criterion first derived by Suydam [7]. Note that the most general pressure profile could be described by allowing α to be a function of r, $\alpha = \alpha(r)$. We have restricted our consideration to constant α in order to reduce the dimension of our parameter space.

The equilibrium fields for such a system are given by

$$B_\theta = r\, B_{\theta o} \exp\{-\int_o^r \frac{[-(\alpha/8k^2)rq'^2 + 2r + d/dr(q^2/2k^2)]}{(q^2/k^2 + r^2)}\, dr\}\ , \tag{2a}$$

$$B_z = qB_\theta/rk\ . \tag{2b}$$

In addition to the overall scale factor $B_{\theta o}$, the equilibrium profiles are seen to depend only on three parameters; the pitch q_o/k, the pressure factor α, and the q exponent σ. We introduce a new parameter, the wall radius b, and extend the definition of the equilibrium fields into a vacuum region surrounding the plasma by setting $q(r) = q'(r) = 0$ for $1<r<b$ and using Eq. (2) to define B_θ and B_z.

In Fig. 1 we plot typical current and magnetic field profiles for force-free, parabolic q-profile configurations with $\alpha = 0$, $\sigma = 1$, and for $q_o/k = 0.5$, 1.0, and 2.0. We note that small values of q_o/k correspond to the toroidal current J_z peaking on the axis. The current is relatively flat for $q_o/k = 1$, while for values $q_o/k > 1$, J_z peaks off the magnetic axis. These profiles change little for finite pressure configurations with $0<\alpha<1$. For configurations with $\alpha = 1$, i.e., with the pressure everywhere at the Suydam limit, the plasma pressure increases as q_o/k (and hence the magnetic shear) is

increased. In Fig. 2 we plot $\beta_\theta \equiv 2\int_o^1 rpdr/\int_o^1 rB_\theta^2\,dr$ vs. q_o/k for $\alpha = 1$, $\sigma = 1$ and for $\alpha = 0.5$, $\sigma = 1$. The total β is approximately equal to one half of β_θ.

The stability of this system to infinite conductivity modes is obtained by minimizing Newcomb's form of the energy integral,

$$W = \frac{\pi}{2}\int_o^b dr\ \left[f\left(\frac{d\xi}{dr}\right)^2 + g\xi^2\right] , \tag{3}$$

where the functions f and g are defined as

$$f = rB_\theta^2\,\frac{(1-nq)^2}{\left(1+n^2k^2r^2\right)} , \tag{4a}$$

$$g = \frac{n^2k^2rB_\theta^2}{\left(1+n^2k^2r^2\right)}\left[-\frac{\alpha q'^2}{4k^2} + (1-nq)^2 + \frac{2\left(n^2q^2-1\right)}{\left(1+n^2k^2r^2\right)}\right] . \tag{4b}$$

Here, the perturbations vary as $\xi(r,\theta,z) = \tilde{\xi}(r)\exp(i\theta - inkz)$, so that n is the longitudinal (or toroidal) mode number and a poloidal mode number of $m \equiv 1$ is explicitly assumed, as it is known to be the most unstable.

Following the prescription of Newcomb [8], we integrate the Euler-Lagrange equation

$$\frac{d}{dr}\left(f\,\frac{d\xi}{dr}\right) - g\xi = 0 , \tag{5}$$

in each independent subinterval bounded by the physical boundarys $r = 0$, $r = b$, and/or by the mode rational surface, $q = 1/n$. A solution which is "small" at one endpoint and which vanishes anywhere in a subinterval signifies an unstable mode. Examination of the functional forms of f and g in Eq. (4)

reveals that each stability calculation depends on the toroidal mode number n only through the combinations nq and nk.

A general analysis of the destabilizing terms in Eqs. (3) and (4) has been given by Robinson [9]. Here we only note that both the first and the third terms in the bracket of Eq. (4b) can contribute to instability. When the first term, which is proportional to the pressure parameter α, dominates, we call the mode pressure driven. When the combined second and third terms dominate, which requires $nq_o \lesssim 1$, we call the mode current driven. We proceed to treat α, σ, b, nk, nq_o as parameters and evaluate stability numerically according to the proceedure outlined above.

The reduction of the equilibrium and stability problem to a small number of parameters allows one to graphically identify stable operating regimes as is done in Figs. 3 and 4. Figure 3 maps out the stable regions in (nk, nq_o) space for $\sigma = 1$, $\alpha = 0.0$, 0.5, 1.0, and b = 1.0, 1.5, and 2.0. An equilibrium configuration on these diagrams corresponds to a straight line eminating from the origin with fixed q_o/k. If the entire line lies in the stable region, the equilibrium is stable to all ideal modes.

The first thing one notices upon examining Fig. (3a) is that force free equilibrium ($\alpha = 0$) with a wall on the surface of the plasma (b = 1) and with $q_o/k < 0.67$ are unstable to internal current driven modes. This also follows from examining the Euler-Lagrange equation around the origin of a zero pressure equilibrium with $nq_o = 1$. Equation (5) becomes, for $r \ll 1$,

$$\frac{1}{4}\left(q_o/k\right)^2 \frac{d}{dr}\, r^7 \frac{d\xi}{dr} + r^5\xi = 0 \ . \tag{6}$$

If we expand ξ in a Taylor series about the origin, the condition that the roots of the indicial equation be real and unequal is that $q_o/k < 2/3$, which

is in agreement with Fig. 3(a) and with Robinson [9].

As the pressure is increased from zero, Figs. 3(b) and 3(c), the upper right hand corner of these diagrams become unstable, indicating finite n pressure driven instabilities with the mode rational surface in the plasma, $nq_o > 1$. From Figs. 2 and 3(c), one sees that there exists stable configurations with the wall on the surface of the plasma, b = 1, with pressure parameter $\alpha = 1$, and with pitch $q_o/k = 1.1$, corresponding to a volume averaged β_θ of about 38%.

Examination of Figs. 3(d) through 3(i) shows that as the wall is removed from the surface of the plasma, i.e., as b becomes greater than unity, the region of instability due to the pressure driven modes increases, while that due to the current driven modes remains about the same. However, from Fig. 3(e), we see that a configuration with wall radius b = 1.5, pressure parameter $\alpha = 0.5$, and pitch $q_o/k = 2.0$ is stable to all ideal modes. From Fig. 2, this corresponds to $\beta_\theta \simeq 70\%$.

It is evident from Figs. 2 and 3 that the maximum stable β configuration for a fixed pitch q_o/k and wall radius b does not in general have the pressure parameter α equal to unity, although this is the case for b = 1 and $0.67 < q_o/k < 1.1$. For large enough values of the pitch parameter q_o/k, the maximum stable β approaches a limit of $\beta_\theta \simeq 70\%$. This limit is reached at $q_o/k \simeq 2.0$ for b = 1 and b = 1.5, where it corresponds to a value of $\alpha \simeq 0.5$. For b = 2 the limit is reached at $q_o/k \simeq 2.6$ where it corresponds to a value of $\alpha \simeq 0.3$.

Figures 1 through 3 were for the exponent parameter σ in the q profile equal to 1. Raising σ above 1 has little effect on the stability diagrams except for in the vicinity of $nq_o = 1$. In Fig. 4 we show the analogue of Fig. 3(a), but with $\sigma = 2$. We see that for all values of q_o/k there is a narrow region of instability to current driven modes for $nq_o \sim 1$.

An approximate condition for instability can be derived which reproduces the structure of Fig. 4 for $\sigma > 1$. We consider $\sigma = 2$ and values of q_o slightly less than a rational number, so that $nq = (1-\varepsilon)(1-r^4)$, where $\varepsilon << 1$. The Euler equation, (5), evaluated near the origin where $r << 1$ and $B_\theta \sim B_{\theta o} r$ becomes

$$\frac{d}{dr}\, r^3(\varepsilon+r^4)^2\, \frac{d\xi}{dr} + 4n^2k^2r^3(\varepsilon+r^4)\xi = 0 \ . \tag{7}$$

This is readily solved by a power series expansion. If we take $\xi = \sum_{m=o}^{\infty} \xi_m \left(n^2k^2r^2/\varepsilon\right)^m$, then one obtains the recursion relation

$$\xi_{m+1} = \frac{-2}{(m+1)(2m+4)} \left[\xi_m + (m-1)(2m+4)y\, \xi_{m-1} + y\, \xi_{m-2} \right.$$

$$\left. + y^2\, \frac{(2m+4)(m-3)}{2}\, \xi_{m-3}\right]$$

with $y \equiv \varepsilon/n^4k^4$. The first few ξ_m are given by $\xi_o = 1$, $\xi_1 = -1/2$, $\xi_2 = 1/12$, $\xi_3 = -(1-36y)/144$, $\xi_4 = (1-204y)/2880$. Evaluation of this series shows a zero for $y \leq 0.017$ at $n^2k^2r^2/\varepsilon = 4.7$, indicating instability for $(1-nq_o) < 0.017\, n^4k^4$. This is in good agreement with Fig. 4.

III. TOROIDAL RESULTS

The investigation of the stability properties of the toroidal spheromak with arbitrary shape and equilibrium profiles necessitates using large computer programs to calculate equilibrium and linear ideal MHD stability. A description of these programs and their convergence properties has been given previously [10-12]. Here, we concentrate on presenting and understanding their results.

As in Ref. [13], we parameterize the shape of the equilibrium we study as illustrated in Fig. 5. Motivated by the exact spherical solution, the outer boundary, in spherical coordinates, is given by $r \sin\theta\, j_1(r)\, P_1^1(\cos\theta) + \delta = 0$, where $0 < \delta < 1.063$ measures the size of the "flux hole." To "flatten" (oblate) the configuration, we multiply the z coordinate by $[1+\varepsilon]^{-1/2}$.

The parameters δ and ε therefore determine the shape of the outermost flux surface. In analogy with the cylindrical study, we take the safety factor profile to be of the form $q(\Psi) = q_o[1-(\Psi/\Psi_o)^\sigma]$, where $0 < (\Psi/\Psi_o) < 1$ is the normalized poloidal magnetic flux. The pressure profile, $p(\Psi)$, is taken to be a fraction, α, of the pressure $p_m(\Psi)$ that is everywhere marginally stable to the Mercier criterion [14] for marginal stability to ideal interchange modes in a torus. Thus $p(\Psi) = \alpha\, p_m(\Psi)$ where $0 \leq \alpha \leq 1$ and

$$D_I \equiv F\left(\frac{dp_m}{d\Psi}\right)^2 + (E+H)\left(\frac{dp_m}{d\Psi}\right) - \frac{1}{4} = 0 \quad . \tag{8}$$

Here,

$$F \equiv \frac{(2\pi)^2}{q'^2}\left[\left\langle \frac{R^2}{|\nabla\Psi|^2} \right\rangle \left\langle \frac{B^2}{|\nabla\Psi|^2} \right\rangle - R^2 B_T^2 \left\langle \frac{1}{|\nabla\Psi|^2} \right\rangle^2 \right],$$

$$H \equiv \frac{-2\pi R B_T}{q'}\left[\frac{1}{\langle B^2 \rangle} \left\langle \frac{B^2}{|\nabla\Psi|^2} \right\rangle - \left\langle \frac{1}{|\nabla\Psi|^2} \right\rangle \right],$$

$$E \equiv \frac{1}{q'^2} \left\langle \frac{B^2}{|\nabla\Psi|^2} \right\rangle \left[\frac{2\pi q' R B_T}{\langle B^2 \rangle} - \left(\frac{1}{\Psi'} \right)' \right].$$

In these expressions, prime denotes differentiation with respect to the volume within a flux surface, R is the major radius, B_T is the toroidal field strength, $B^2 = |\nabla\Psi|^2/(2\pi R)^2 + B_T^2$, and brackets denote flux surface averages.

Once the plasma equilibrium is known, Eq. (8) is solved as a quadratic

equation for $(dp_m/d\Psi)$ on each flux surface. Since the pressure gradient enters into the equilibrium equation, Eq. (8) must in practice be solved by numerically iterating its solution with the solution to the Grad-Shafranov equation

$$(2\pi)^{-2} R^2\nabla\cdot(R^{-2}\nabla\Psi) + R^2 \frac{dp}{d\Psi} + \frac{(2\pi)^2 q}{\langle x^{-2}\rangle}\left[\frac{\Psi' q}{\langle x^{-2}\rangle}\right]' = 0 \ . \qquad (9)$$

The equilibrium is therefore defined by the parameters $\varepsilon,\delta,q_o,\sigma$, and α. A stability calculation also requires the specification of the toroidal mode number n and the spheromak wall separation parameters a_ω and b_ω, Fig. 6.

To illustrate the range of current distributions considered, we plot in Fig. 7 the poloidal magnetic flux surfaces and the midplane current profiles for three equilibrium configurations with $\varepsilon = 2$, $\delta = 0.1$ $\sigma = 1$, $\alpha = 0$, and with $q_o = 0.2$, 0.35, and 1.35. As in Fig. 1, we see that small values of q_o correspond to the toroidal current being very peaked, while large values of q_o correspond to flat or hollow toroidal current profiles. In analogy to Fig. 2, we plot in Fig. 8 β_θ vs. q_oR/a for configurations with $\alpha = 1$ (i.e., pressure everywhere at the Mercier limit), $\sigma = 1$ (linear q profiles), and for various values of the shaping parameters ε and δ. Here β_θ is defined by

$$\beta_\theta = -\int_o^{\Psi_o} p(\Psi)V(\Psi)d\Psi \Big/ \int_o^{\Psi_o} V(\Psi)\left[p' + \langle R^{-2}\rangle\left(RB_T\right)'\right] d\Psi \ ,$$

where V is the volume within a constant Ψ surface. As in the cylinder, β_θ set by the interchange limit increases with q_oR/a. In addition, we note that for configurations with the same values of q_oR/a the value of β_θ increases with ε, or oblateness.

Figures 9 through 11 summarize the results of over 1000 stability calculations on over 100 different toroidal equilibrium configurations. Each

symbol indicates stability or instability to a particular mode with toroidal mode number n = 1, 2, or 3. These were all performed with the q exponent σ = 1, so that $q(\Psi) = q_o[1-(\Psi/\Psi_o)]$. Two values of the flux hole δ were used, δ = 0.1 which corresponds to aspect ratio R/a = 1.3, and δ = 0.3 which corresponds to aspect ratio R/a = 1.6. Each figure corresponds to a different value of the elongation parameter ε. Figure 9 with ε = 0 is the most elongated (prolate), Fig. 10 with ε = 2 corresponds to nearly circular flux surfaces, and Fig. 11 with ε = 4 is the least elongated (the most oblate). The corresponding cylindrical stability boundaries of Fig. 3 are drawn on each figure for comparison.

We plot typical eigenfunctions, as determined by the PEST-II toroidal stability code [12], in Figs. 12 and 13. Figure 12 illustrates the eigenfunction of a n = 2 current driven mode with the wall at the surface of the plasma Fig. 12(a), and with the wall removed to infinity Fig. 12(b). These equilibrium have q_o = 0.45, α = 0, δ = 0.1, and ε = 0. The eigenfunction for both these modes consists of primarily a poloidal mode number m = 1 harmonic which does not resonate with the perturbation since $m - nq_o$ is greater than zero everywhere in the plasma.

In contrast, we plot in Fig. 13 the eigenfunctions for an n = 2 pressure driven instability with the wall on the surface of the plasma, and with α = 1, and δ = 0.3, and ε = 2. As in Fig. 12, and as is also the case with every stability calculation illustrated in Figs. 9 through 11, the poloidal mode number m = 1 harmonic dominates the instability. However, for the pressure driven instabilities in Fig. 13, unlike the current driven instabilities of Fig. 12, the mode rational surface where nq - m = 0 plays a central role in that the eigenfunction is primarily confined to the region nq - m > 0. In Fig. 13(a) where q_o = 0.75 this is the inner one third of the plasma, while in Fig. 13(b) where q_o = 1.05 this is the inner one half.

One of the most striking features one notices about Figs. 9 through 11 is that for a finite wall separation and for modes with $n \geq 2$, there is general qualitative agreement between the toroidal stability results and the corresponding cylindrical results. This agreement is perhaps fortuitous considering the inexact correspondence between the q profiles, where we have used Ψ/Ψ_o as a variable in the toroidal case but r^2 in the cylindrical case, the wall parameters where we have used a_w and b_w in the toroidal case but b/a in the cylinder, and have the pressure determined as a fraction of the Mercier limit in the torus vs. the Suydam limit in the cylinder.

Examination of the figures does reveal, however, qualitative differences between the stability of the $n = 1$ and $n = 2$ modes in the cylinder and the torus. As discussed in detail in Ref. [13], and shown in parts (g) through (i) of Figs. 9 through 11, the $n = 1$ modes are always unstable in a torus in the absence of a conducting wall. They arise from the fact that unlike a cylinder, an externally imposed vertical magnetic field is needed to maintain equilibrium in toroidal geometry. The plasma has a tendency to tilt so as to align its magnetic moment with the external field, or to shift horizontally into a region of weaker magnetic field strength [13].

Figures 9(g), 10(g), and 11(g) indicate that the $n = 2$ mode is also always unstable in the torus in the absence of a conducting wall. The eigenfunction for this mode corresponds to the plasma ring deforming into the shape of a baseball seam. Since this mode, like the $n = 1$ tilt and shift modes is current driven and absent in the cylinder, it is presumably also driven by the interaction between the plasma current and the externally supplied magnetic field. From Figs. 9(d), 10(d), and 11(d) we see that this $n = 2$ bending mode will be stabilized by the presence of a spherical conducting wall with a mean separation of a half of a plasma minor radius.

Examination of Figs. 9(a), 10(a), and 11(a) shows that even for a pressureless plasma with a wall on its surface, there can be an internal n = 1 current driven instability of the torus if $q_o > 1$. Closer numerical evaluation of the stability boundary for this mode indicates that it goes unstable at exactly $q_o > 1$. This internal kink mode, which from Fig. 3 can be seen to be stable in the cylinder, is apparently caused by toroidal coupling of the m = 1 and m = 2 poloidal harmonics.

That the internal kink mode can be unstable in the toroidal spheromak when $q_o > 1$ is consistent with analysis [15,16]. It was found that the stability of a circular cross section torus can be determined by solving a homogeneous equation for the m = 2 harmonic amplitude x_2,

$$\frac{d}{dr}\left[r^3\left(q^{-1} - \frac{1}{2}\right)^2 \frac{dx_2}{dr} \right] - 3r\left(q^{-1} - \frac{1}{2}\right) x_2 = 0 \ . \tag{10}$$

If r_s is the radius of the q = 1 surface, and if x_{2i} and x_{2e} are the solutions of Eq. (10) which satisfy the left and right boundary conditions, respectively, one defines the parameters

$$b = \frac{r_s}{4} \frac{d}{dr} \ln \frac{x_{2i}}{r} \bigg|_{r_s} \ , \quad c = \frac{r_s}{4} \frac{d}{dr} \ln x_{2e} r^3 \bigg|_{r_s} \ , \tag{11}$$

$$\beta_p = \frac{-2}{B_\theta^2(r_s) r_s^2} \int_o^{r_s} r^2 \frac{dp}{dr} \, dr \ ,$$

$$s = \frac{1}{r_s^4} \int_o^{r_s} r^3 \left[q^{-2} - 1\right] dr \ .$$

Stability is then determined by the condition [16]

$$\delta W = \frac{8s(1+b-c)+9b(1-c)-24bc(s+\beta_p)-16c(1+b)(s+\beta_p)^2}{(1+b-c)} > 0 \quad . \tag{12}$$

We have plotted in Fig. 14 the stability boundary defined by Eq. (12) for a spheromak profile with $q = q_o[1 - (r/r_w)^2]$, as well as for a tokamak profile with $q = q_o[1 + (r/r_w)^2]$ for comparison. The spheromak and the tokamak case are seen to be opposites. The internal kink in the tokamak is unstable in cylindrical geometry, stable at zero pressure in a torus, but unstable in the torus above some critical pressure. The internal kink in the spheromak is stable in cylindrical geometry, unstable at zero pressure in the torus, but stable in the torus above the same critical pressure. Unfortunately, stabilization of this mode by operating at a large value of $\beta_p(r_s)$ appears impractical since this would violate the maximum p' criterion set by the Mercier criterion, Eq. 8.

As in the cylindrical configuration illustrated in Fig. 4, a q profile with low shear at the origin, $dq_c/d\psi = 0|_{\psi=0}$, can lead to instability in toroidal geometry if q_o is sufficiently close to a rational surface, $q_o \lesssim 1/n$. This phenomena is illustrated in Figs. 15 and 16 where we present the stability results of a sequence of toroidal low shear zero pressure equilibrium with $q = q_o(1 - \psi^4)$. Figure 15 has the shape parameter $\varepsilon = 2$ and shows that the width of this unstable region around the $q = 1/2$ surface increases with the flux hole δ (or the aspect ratio R/a). Figure 16 has the flux hole $\delta = 0.1$ and shows that the width of this unstable region increases with decreasing ε.

Beta optimization in toroidal geometry is illustrated in Fig. 17 where we plot the maximum β_θ stable to internal modes versus $q_o R/a$ for a variety of outer flux surface shapes. Each curve is qualitatively similar to the curve

marked b = 1 in Fig. 2 for cylindrical geometry. For low values of q_oR/a, the pressure is limited by the internal current driven modes. As q_oR/a is increased, there is a region in which β_θ is limited by marginal stability to interchange modes. For the oblate configurations with $\epsilon = 2$ and $\epsilon = 4$, when $q_oR/a \gtrsim 1$ the maximum stable β_θ limit is set by stability to the internal pressure driven modes.

However, unlike the cylindrical geometry of Fig. 2, the ultimate β_θ limit for each curve is set by the limit that $q_o \leq 1$ for stability to the n = 1 internal kink mode. This new limit is seen to favor configurations with large aspect ratios, or equivalently, large values of the flux hole δ. Also, it is seen that the maximum stable β_θ increases with the oblateness parameter ϵ, although this increase is more modest when increasing ϵ from two to four than it is when increasing ϵ from zero to two.

So far we have made no mention of infinite n ballooning modes or zero n axisymmetric modes in the torus. The equilibrium configurations we have chosen to look at are manifestly stable to the Mercier criterion, Eq. (8). We have applied the ballooning criterion [17] to these equilibrium and have found them all to be stable to this criterion. This result is consistent with the study of Greene and Chance [18] in which they found that equilibrium configurations with monotonically decreasing q-profiles and which are everywhere stable to the Mercier criterion are also stable to the ballooning criterion.

The axisymmetric n = 0 modes, however, are potentially unstable in toroidal geometry. These modes arise from the interaction of the plasma toroidal current with the gradients of the externally applied equilibrium magnetic fields. The criterion for infinite wall stability of these modes in the spheromak is the same as that in the tokamak, i.e., that the external field have a favorable curvature [19], or equivalently, that the plasma shape

be sufficiently oblate, $\varepsilon \gtrsim 2$. For configurations with $\varepsilon \lesssim 2$, a conducting wall separated on the order of a minor radius should provide passive stabilization of these modes.

IV. SUMMARY AND CONCLUSIONS

We have mapped out the ideal magnetohydrodynamic stability boundaries of the spheromak configuration. A useful model with a reduced parameter space was obtained by examining the cylindrical spheromak. This predicted unstable current driven internal modes if the value of the pitch on axis is too low, $q_o/k \lesssim 0.67$ or if the shear at the origin is too low, i.e., $q = q_o(1 - r^{2\sigma})$ with $\sigma > 1$. The local criterion for interchange mode stability set an upper limit on the pressure gradient everywhere. Configurations that are everywhere marginally stable to interchange modes will be stable to internal pressure driven low-n modes if $q_o/k \lesssim 1.1$. This corresponds to a maximum $\beta_\theta \simeq 38\%$. As the pitch is increased above $q_o/k = 1.1$ the maximum stable β_θ configurations are determined by stability to finite-n pressure driven modes. For $q_o/k \gtrsim 2$, stable configurations exist with the wall separated by half a minor radius and with $\beta_\theta \simeq 70\%$.

By letting q_oR/a be the toroidal generalization of the pitch, the stability boundaries of the toroidal spheromak coincide qualitatively well with those predicted by the cylindrical model with a few exceptions. In toroidal geometry, an internal m = 1, n = 1 kink mode exists whenever $q_o > 1$, while this is not present in the cylinder. Also in toroidal geometry, the presence of the required externally generated vertical field will cause the spheromak to be unstable to n = 2 bending modes and n = 1 modes of either the shift and/or tilt polarity for the wall removed far enough. Recently it has been shown [20] that full conducting walls are not necessary to stabilize these free boundary modes but that nearby passive coils with the figure-eight

and clover-leaf topology should be sufficient to stabilize the n = 1 and n = 2 modes, respectively.

An oblate $\varepsilon = 4$ plasma with a flux hole $\delta = 0.3$ corresponding to an aspect ratio R/a = 1.6 with a conducting wall at its surface will be stable to all internal modes with $q_o = 1.0$ and $\beta_\theta = 65\%$. Removing the conducting wall to an average separation of $a_w = b_w = 1/2$ will cause this configuration to become unstable, however from Figs. 8 and 10(e) we see that a moderately oblate plasma with $\varepsilon = 2$ will be stable to all internal and free boundary modes for $q_o R/a \simeq 1.2$ with $\beta_\theta = 30\%$.

Finally, we remark that these β optimization studies were performed by evaluating stability only to ideal magnetohydrodynamic modes which occur even with infinite conductivity. Consideration of finite-conductivity modes could lead to greatly different conclusions. In fact, since the quantity $D_R = p'[E + (F + H^2)p']$ is greater than zero for all configurations studied here with $p' \neq 0$, we would conclude [21] that the limiting value is $\beta_\theta = 0$. Optimization with respect to these resistive interchange and resistive tearing modes must await a realistic assessment of their nonlinear consequences.

ACKNOWLEDGMENTS

The author wishes to thank D. A. Monticello for aid in generating toroidal equilibrium and R. L. Dewar, R. C. Grimm and J. Manickam for making the PEST-II stability code available. Useful discussions with M. S. Chance, R. L. Dewar, R. C. Grimm, D. A. Monticello, W. Park, D. Robinson, and K. E. Weimer are gratefully acknowledged.

This work was supported by the United States Department of Energy Contract No. DE-AC02-CH03073.

REFERENCES

[1] YAMADA, M., FURTH, H. P., HSU, W., JANOS, A., JARDIN, S. C., OKABAYASHI, M., SINNIS, J., STIX, T. H., and YAMAZAKI, K., Phys. Rev. Lett. 46, (1981) 188.

[2] JARBOE, T. R. et. al., Phys. Rev. Lett. 45 (1980) 1264.

[3] GOLDENBAUM, G. et. al., Phys. Rev. Lett. 44 (1980) 393.

[4] ROSENBLUTH, M. N., BUSSAC, M. N., Nuc. Fusion 19 (1979) 489.

[5] OKABAYASHI, M. and TODD, A. M. M., Nucl. Fusion 20 (1980) 571.

[6] FINN, J., MANHEIMER, W., OTT, E., Phys. Fluids 24 (1981).

[7] SUYDAM, B. R., Int. Conf. Peaceful Uses Atom Energy, Geneva, Vol. 31, p. 157 (1958).

[8] NEWCOMB, W. A., Ann. Phys. 10 (1960) 232.

[9] ROBINSON, D. C., Plasma Phys. 13 (1971) 439.

[10] DELUCIA, J., JARDIN, S. C., TODD, A. M. M., J. Comput. Phys. 37 (1980) 183.

[11] GRIMM, R. C., GREENE, J. M., JOHNSON, J. L. in Methods in Computational Physics, 16 ed. J. Killeen (Academic Press, New York 1973) p 293.

[12] GRIMM, R. C., DEWAR, R. L., MANICKAM, J., CHANCE, M. S., Bull. Am. Phys. Soc. 25 (1980) 864.

[13] JARDIN, S. C., CHANCE, M. S., DEWAR, R. L., GRIMM, R. C., MONTICELLO, D. A., Nucl. Fusion 21 (1981) 1203.

[14] GLASSER, A. H., GREENE, J. M., JOHNSON, J. M., Phys. Fluids 18 (1975) 875.

[15] BUSSAC, M. N., PELAT, R., EDERY, E., SOLE, J. L., Phys. Rev. Lett. 35 (1975) 1633.

[16] ZAKHAROV, L. E., Sov. J. Plasma Phys. 4, (1978) 503.

[17] DOBROTT, D., NELSON, D. B., GREENE, J. M., GLASSER, A. H., CHANCE, M. S., FRIEMAN, E. A., Phys. Rev. Lett. 39 (1977) 943.

[18] GREENE, J. M., CHANCE, M. S., Nucl. Fusion 21 (1981) 453.

[19] YOSHIKAWA, S., Phys. Fluids 7 (1964) 278.

[20] JARDIN, S. C., CHRISTENSEN, U., Princeton Plasma Physics Laboratory Report PPPL-1814 (submitted to Nuc. Fusion).

[21] GLASSER, A. H., GREENE, J. M., JOHNSON, J. L., Phys. Fluids 18 (1975) 875.

Figure Captions

Fig. 1. Equilibrium profiles vs. radius for $\alpha = 0$, $\sigma = 1$. Note that J_z hollows as q_o/k is increased above 1.0.

Fig. 2. Solid curves give β_θ vs. q_o/k for $\alpha = 1$, $\sigma = 1$ and $\alpha = 0.5$, $\sigma = 1$. Dashed curves give maximum β_θ configurations limited by finite-n modes for different wall separations. The total β is approximately given by $\beta = 1/2\ \beta_\theta$.

Fig. 3. Stability boundaries for the cylindrical spheromak with $\sigma = 1$. A given equilibrium corresponds to a straight line eminating from the origin with q_o/k fixed. α is the pressure parameter and b is the wall position.

Fig. 4. A narrow region of instability around $nq_o = 1$, $nk < 1$, exists for $\sigma > 1$.

Fig. 5. Parameterization of the shape of the plasma boundary. ε measures the oblateness, δ measures the size of the flux hole or aspect ratio.

Fig. 6. An ellipsoidal wall is parameterized by the dimensionless numbers a_w and b_w.

Fig. 7. Toroidal and poloidal midplane current profiles and constant poloidal flux Ψ-surfaces for $\varepsilon = 2$, $\delta = 0.1$. Contours are equally spaced in $\Psi^{1/2}$.

Fig. 8. β_θ vs. $q_o R/a$ in toroidal geometry for $\alpha = 1$, $\sigma = 1$, and with shape parameter $\varepsilon = 0$, 2, and 4.

Fig. 9. Stability of modes in a prolate spheromak with $\varepsilon = 0$. Squares correspond to toroidal number $n = 1$ modes, circles to $n = 2$ modes, and triangles to $n = 3$ modes. Solid symbols indicate instability. The wall position is defined as $a_w = b_w = b$.

Fig. 10. Stability of modes in a moderately oblate spheromak with $\varepsilon = 2$.

Fig. 11. Stability of modes in a strongly oblate spheromak with $\varepsilon = 4$.

Fig. 12. Unstable $n = 2$ mode eigenfunction $\xi \cdot \nabla\psi$ versus ψ for (a) fixed boundary mode with wall in contact with plasma and (b) free boundary mode with wall removed to infinity. Equilibrium have $q_o = 0.45$, $\sigma = 1$, $\alpha = 0$, $\delta = 0.1$, and $\varepsilon = 0$. m is the poloidal harmonic number.

Fig. 13. Unstable $n = 2$ mode eigenfunction $\xi \cdot \nabla\psi$ versus ψ for pressure driven mode with (a) $q_o = 0.75$ and (b) $q_o = 1.05$. Equilibrium have $\sigma = 1$, $\alpha = 1$, $\delta = 0.3$ and $\varepsilon = 2$.

Fig. 14. Stability boundaries for the internal kink mode for tokamak-like and spheromak-like profiles.

Fig. 15. Internal mode stability diagram for zero pressure equilibrium with $\varepsilon = 2$ and with low shear at the origin, $q = q_o[1 - (\Psi/\Psi_o)^4]$.

Fig. 16. Internal mode stability diagram for zero pressure equilibrium with $\delta = 0.1$ and with low shear at the origin, $q = q_o[1 - (\Psi/\Psi_o)^4]$.

Fig. 17. Beta limits for internal mode stability of the toroidal spheromak with $\sigma = 1$. Below point A, beta is limited by internal current driven modes. Between A and B, limit is set by Mercier criterion. Above point B, n = 2 internal pressure driven modes limit beta.

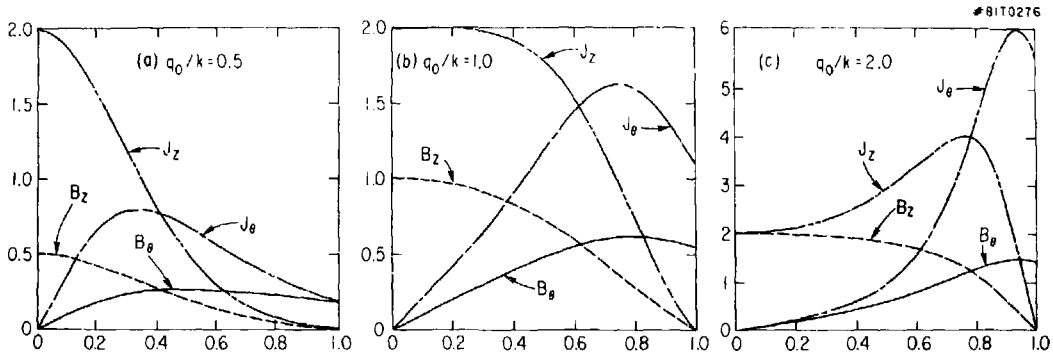
#81T0276
(a) $q_0/k = 0.5$
(b) $q_0/k = 1.0$
(c) $q_0/k = 2.0$
J_z
B_z
J_θ
B_θ
0
0.2
0.4
0.6
0.8
1.0
0.5
1.0
1.5
2.0
2
3
4
5
6

Fig. 1

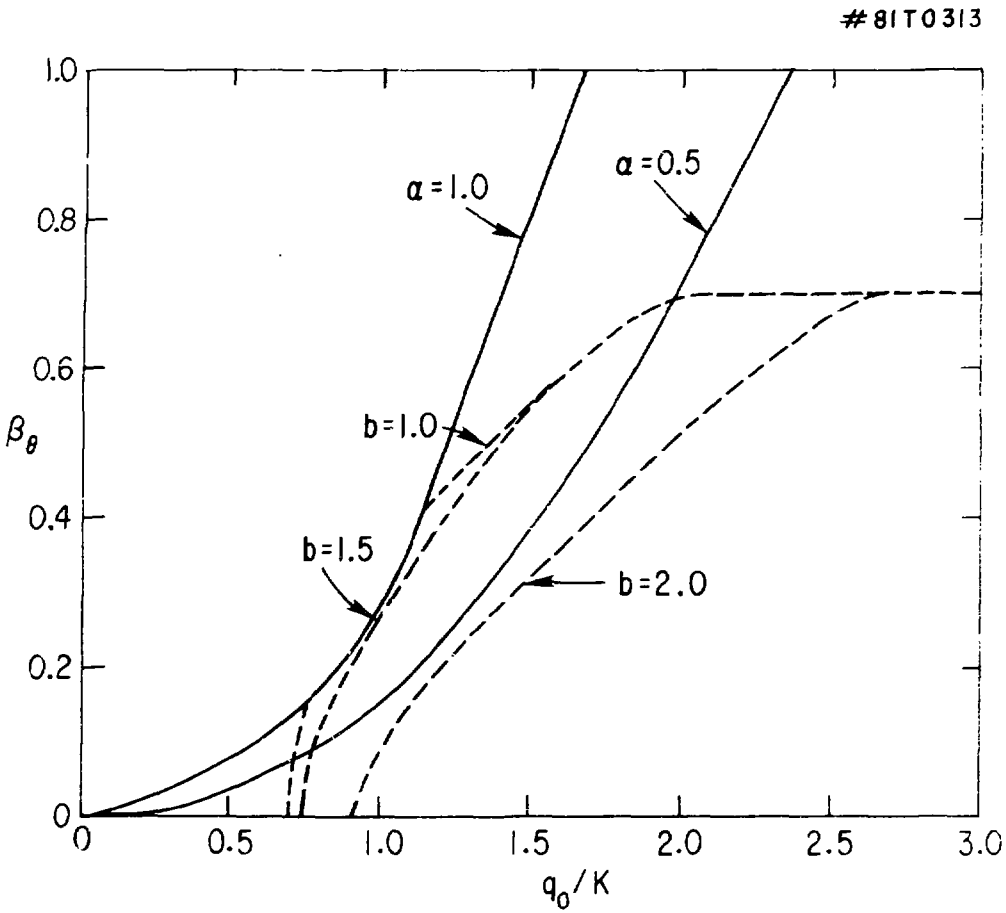
#81T0313
1.0
0.8
0.6
0.4
0.2
0
β_θ
α = 1.0
α = 0.5
b = 1.0
b = 1.5
b = 2.0
0
0.5
1.0
1.5
2.0
2.5
3.0
q_0/K

Fig. 2

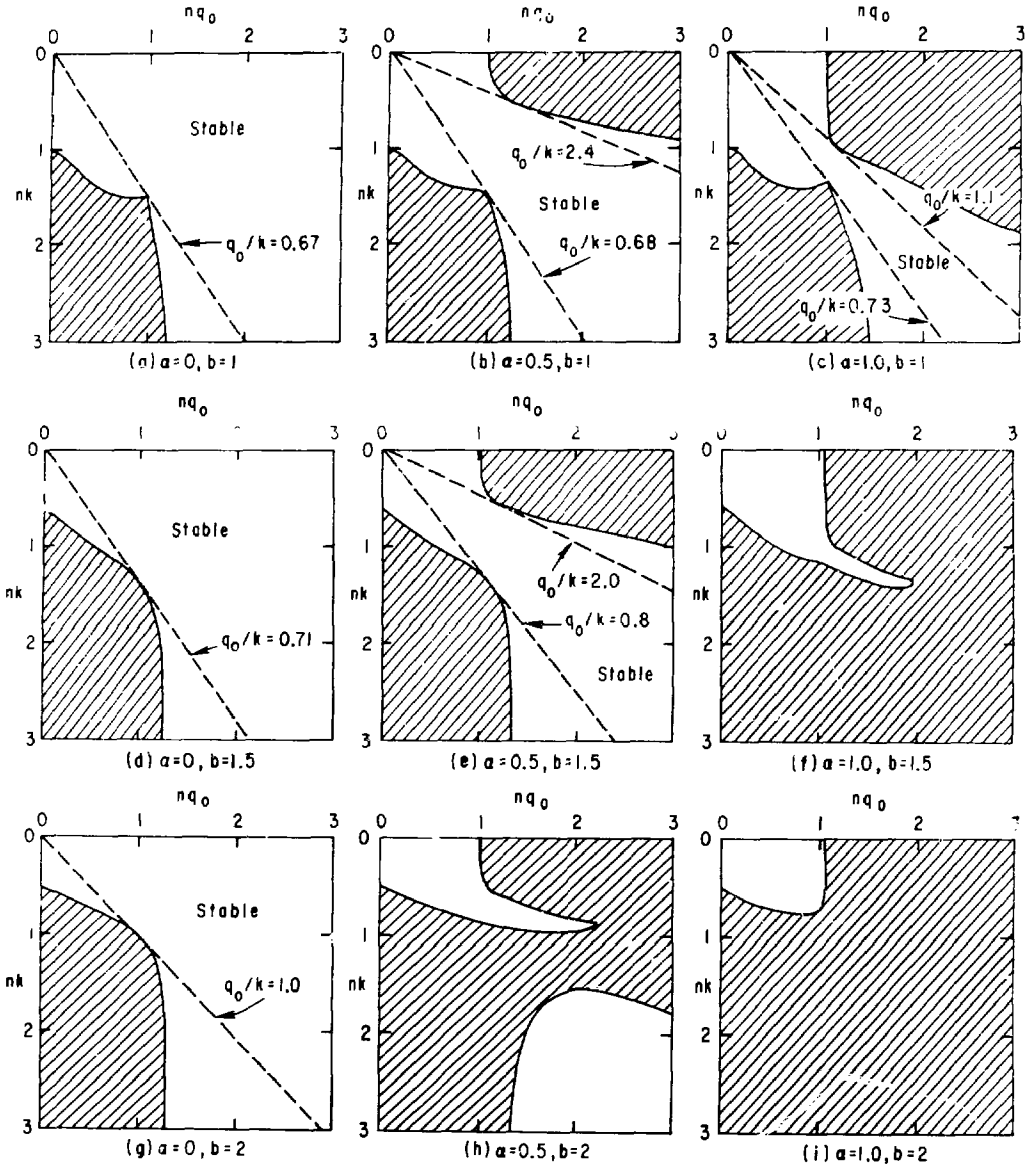
nq0
nk
Stable
q0/k=0.67
(a) α=0, b=1
q0/k=2.4
Stable
q0/k=0.68
(b) α=0.5, b=1
q0/k=1.1
Stable
q0/k=0.73
(c) α=1.0, b=1
Stable
q0/k=0.71
(d) α=0, b=1.5
q0/k=2.0
q0/k=0.8
Stable
(e) α=0.5, b=1.5
(f) α=1.0, b=1.5
Stable
q0/k=1.0
(g) α=0, b=2
(h) α=0.5, b=2
(i) α=1.0, b=2

Fig. 3

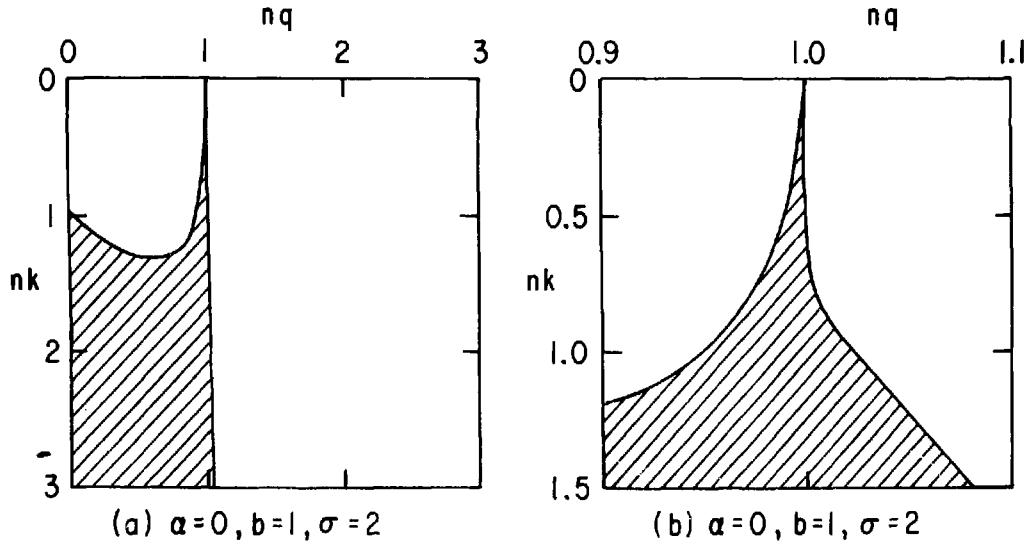

Fig. 4

81T0048

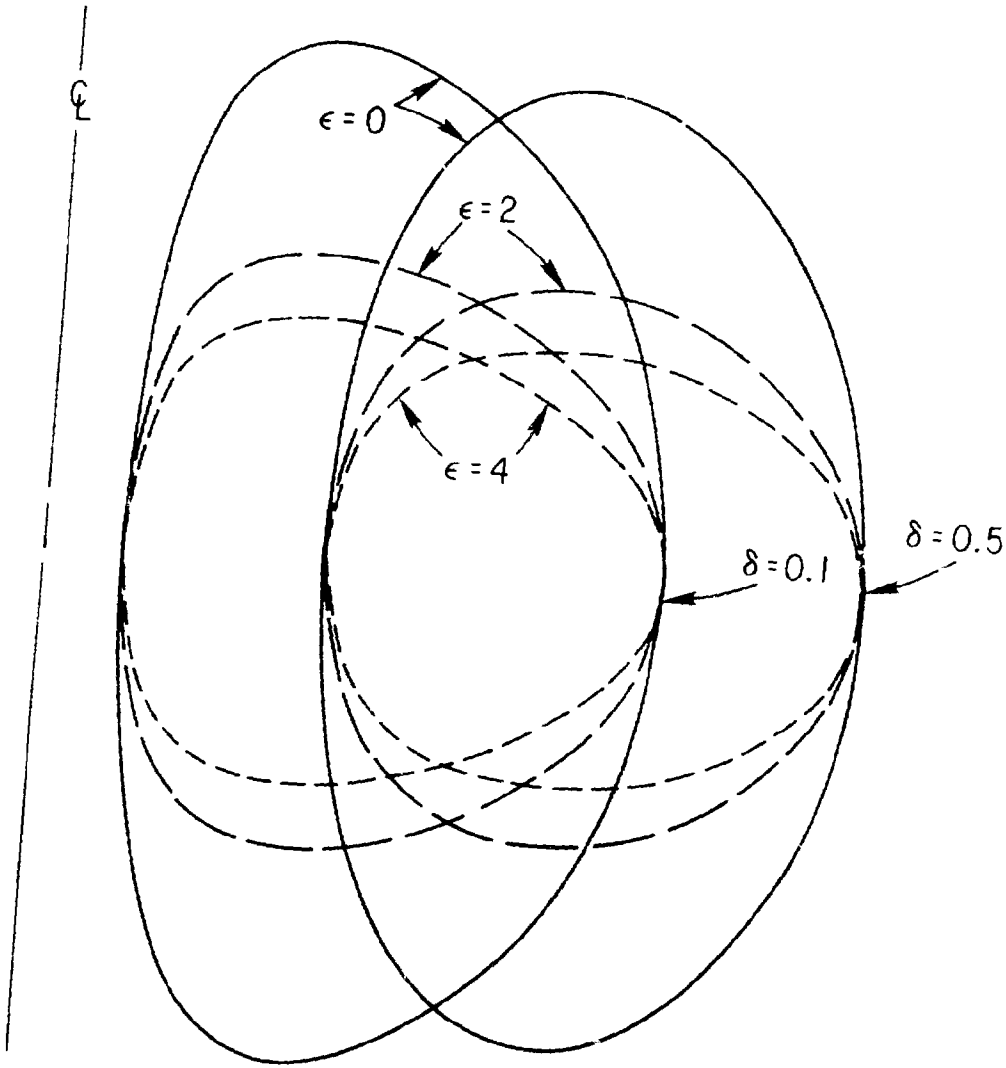

Fig. 5

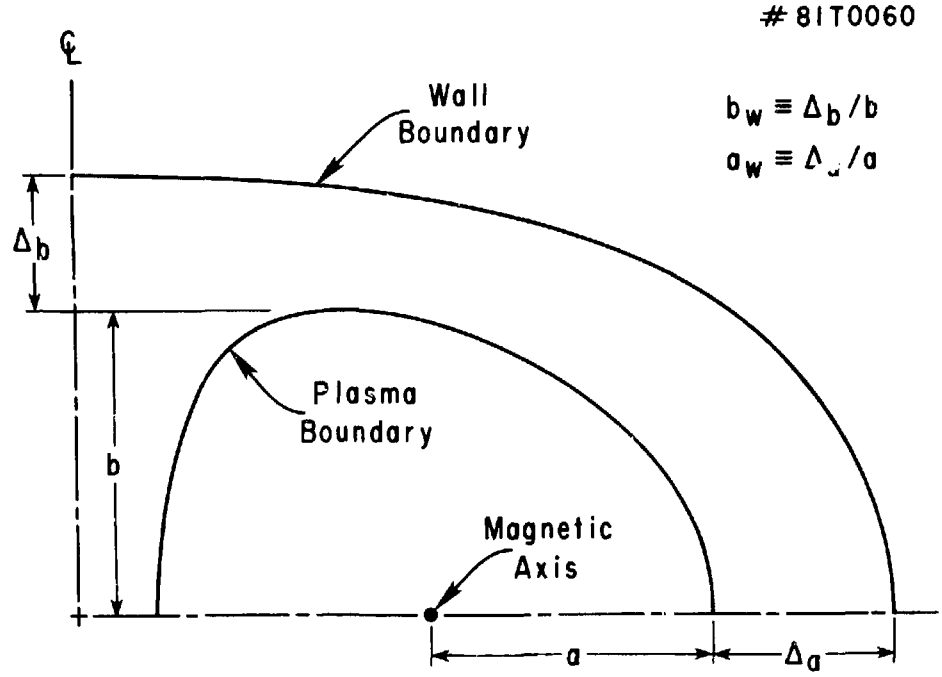
#81T0060
℄
Wall
Boundary
$b_w \equiv \Delta_b / b$
$a_w \equiv \Delta_a / a$
Δ_b
b
Plasma
Boundary
Magnetic
Axis
a
Δ_a

Fig. 1

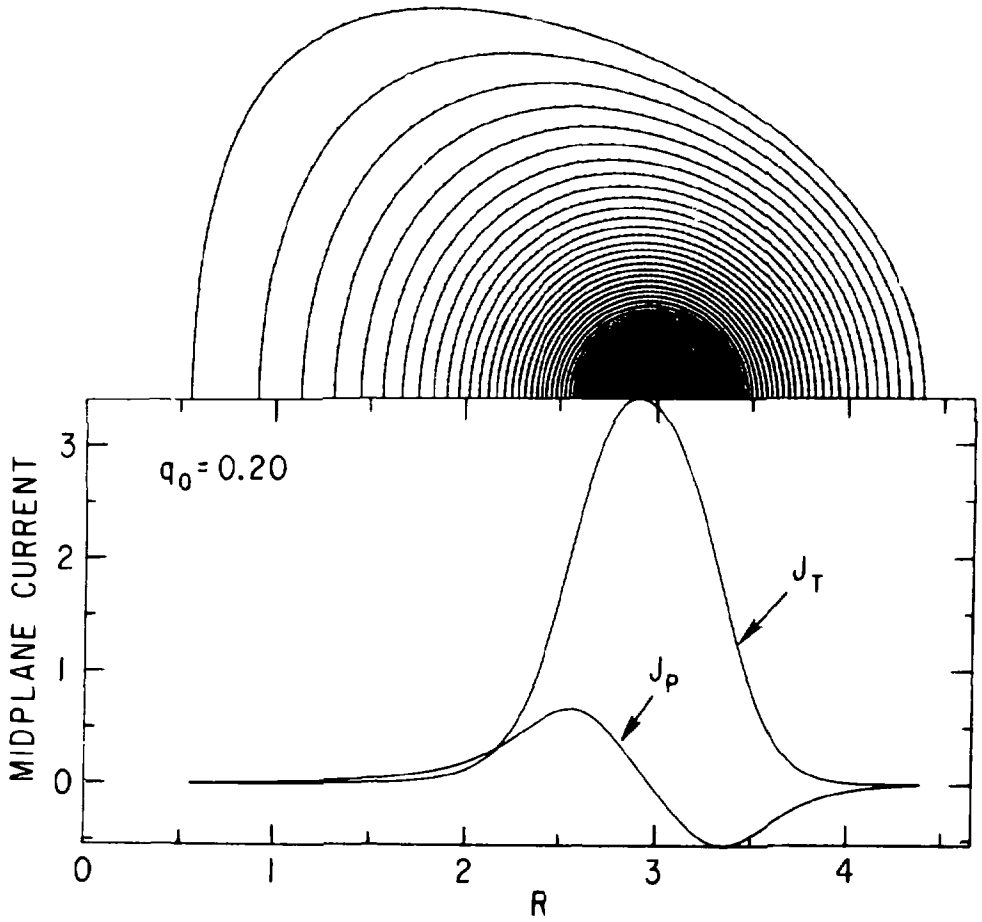

Fig. 7a

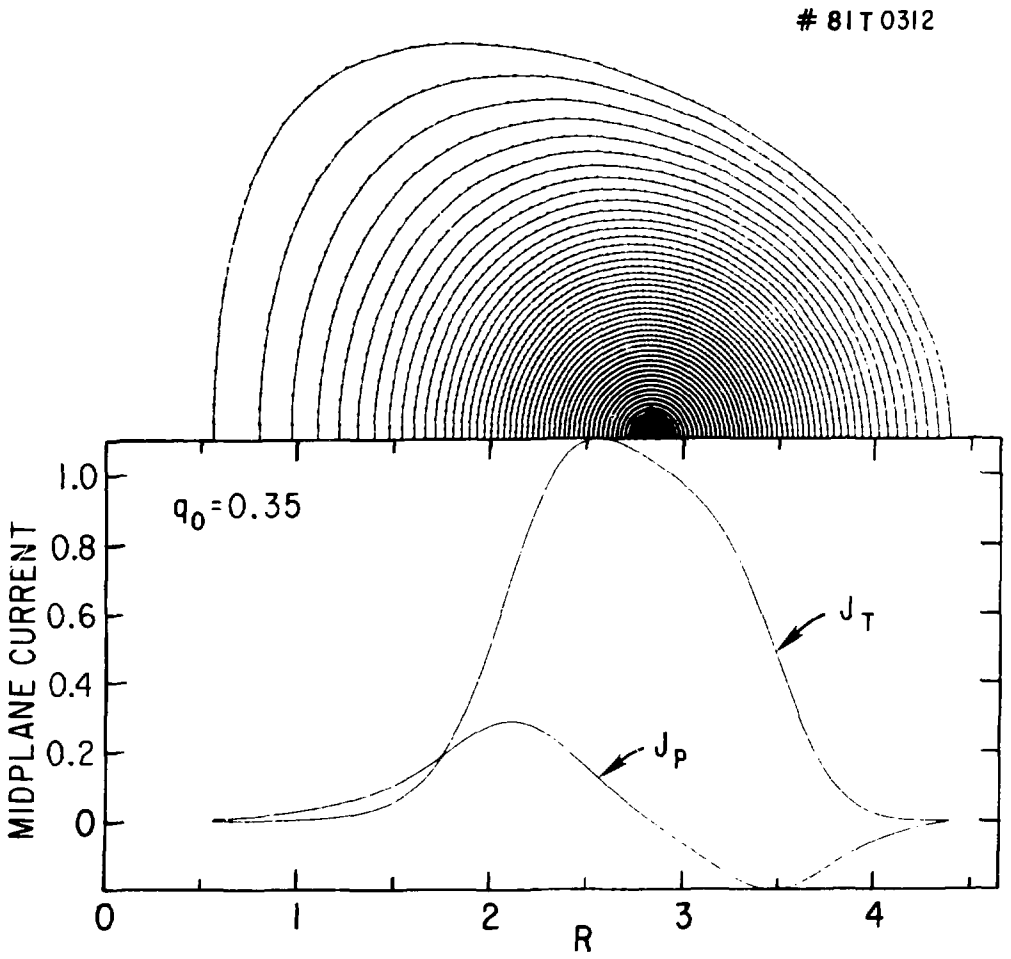

Fig. 7b

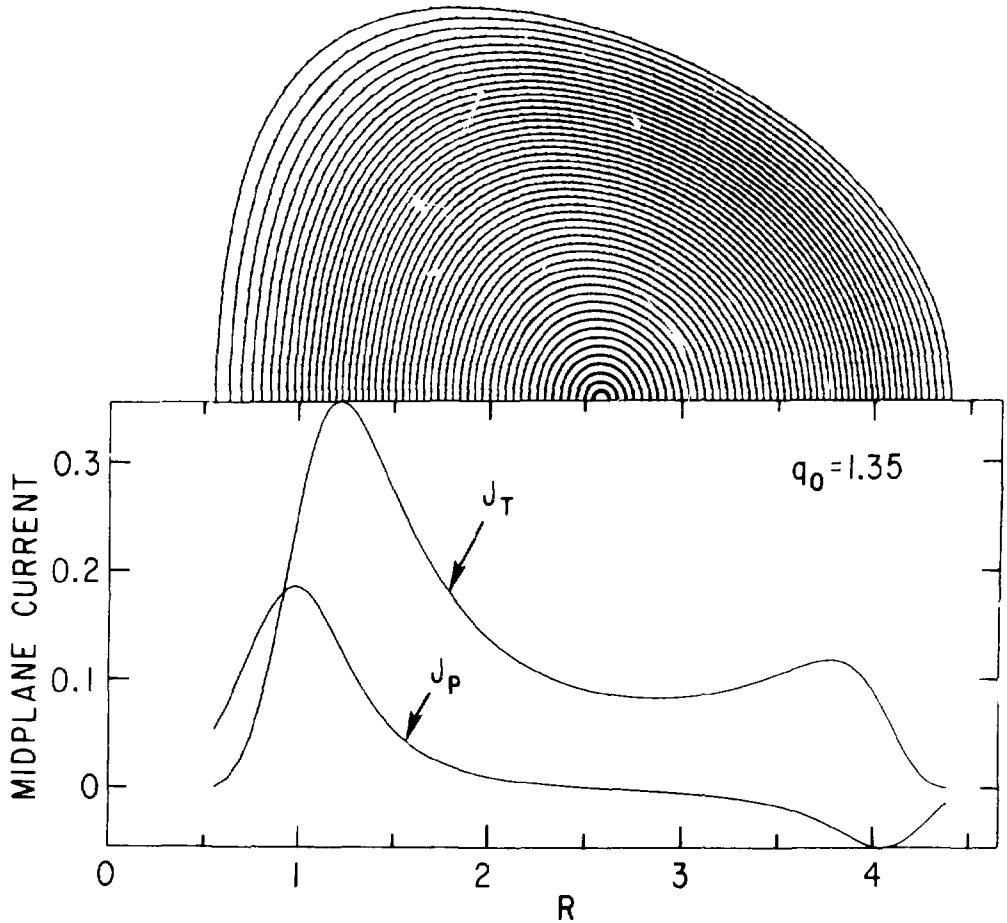

Fig. 7c

#81T0306

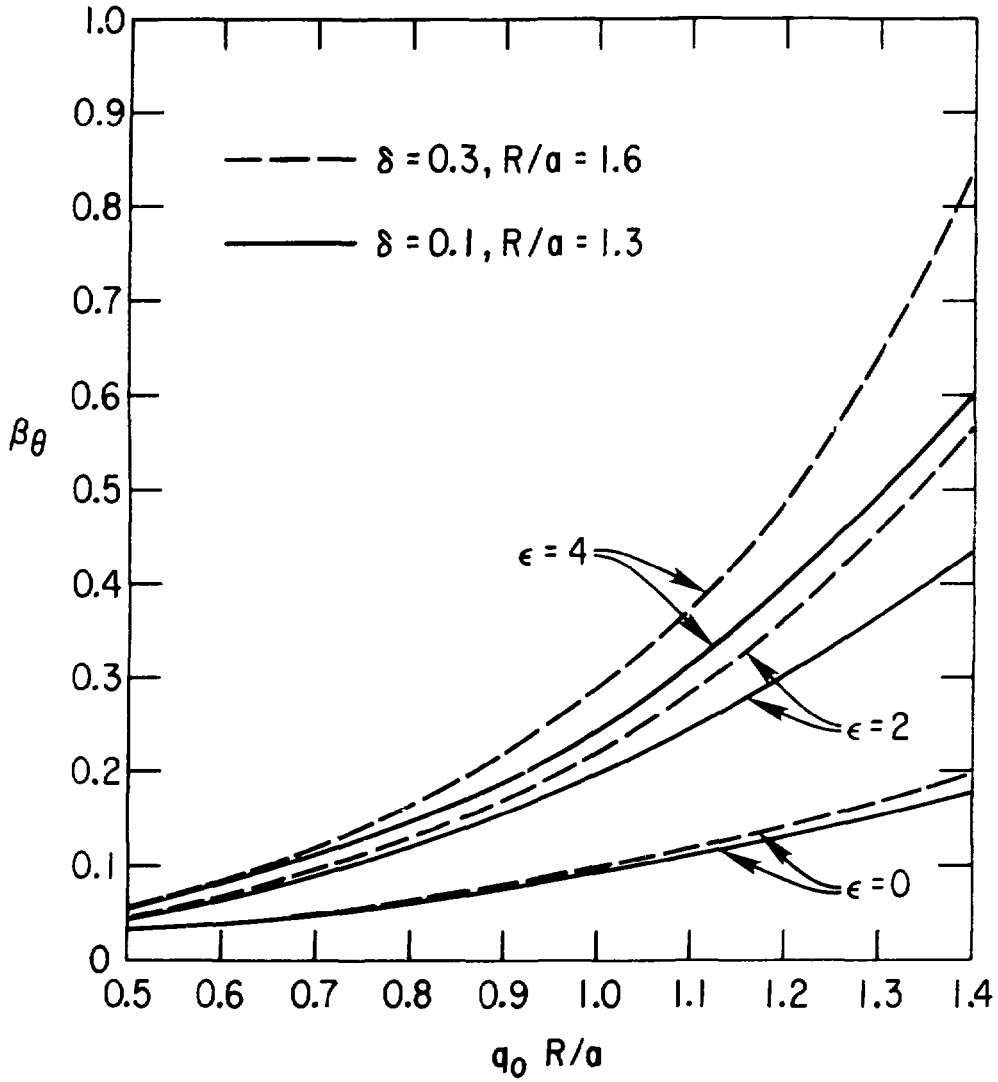

Fig. 8

#8170316

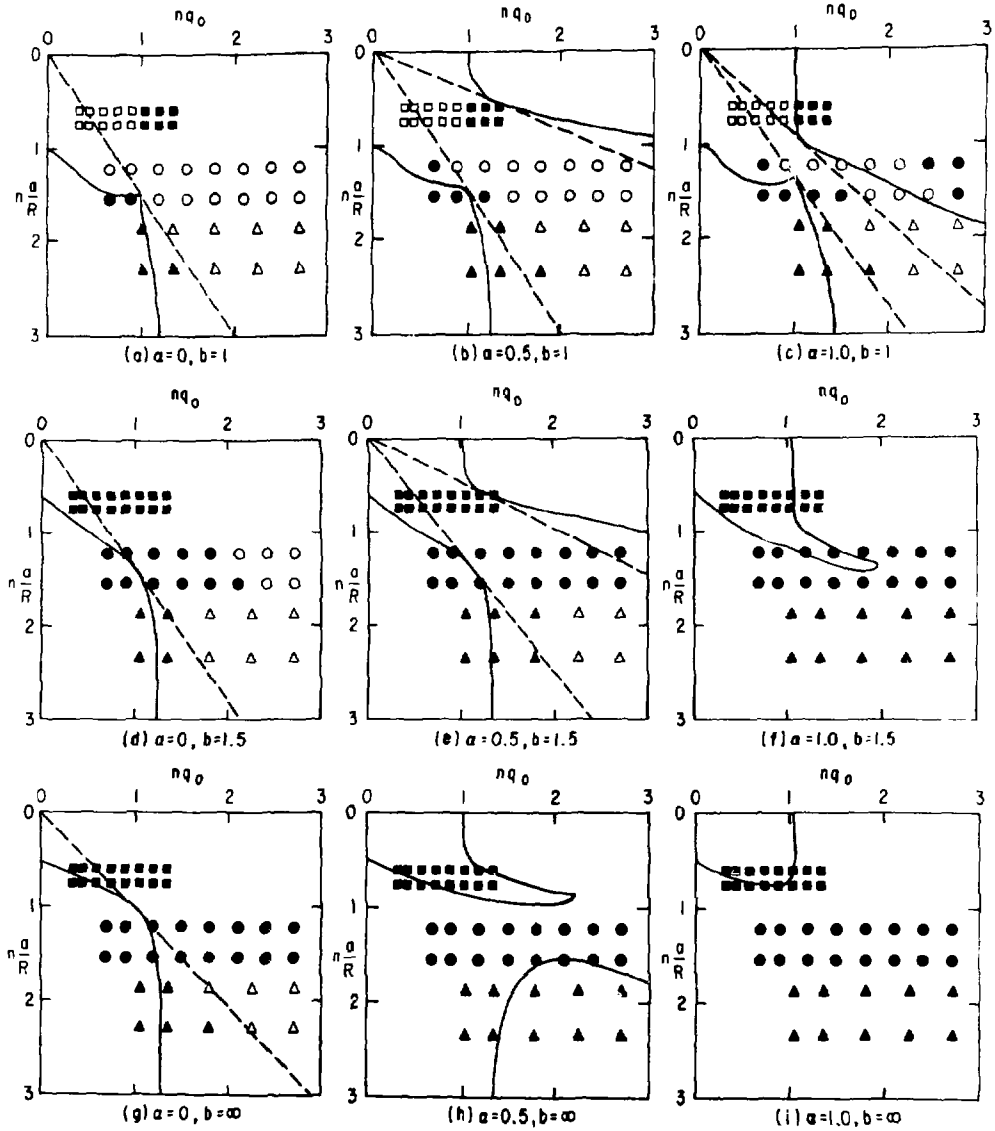

Fig. 9

#81T0318

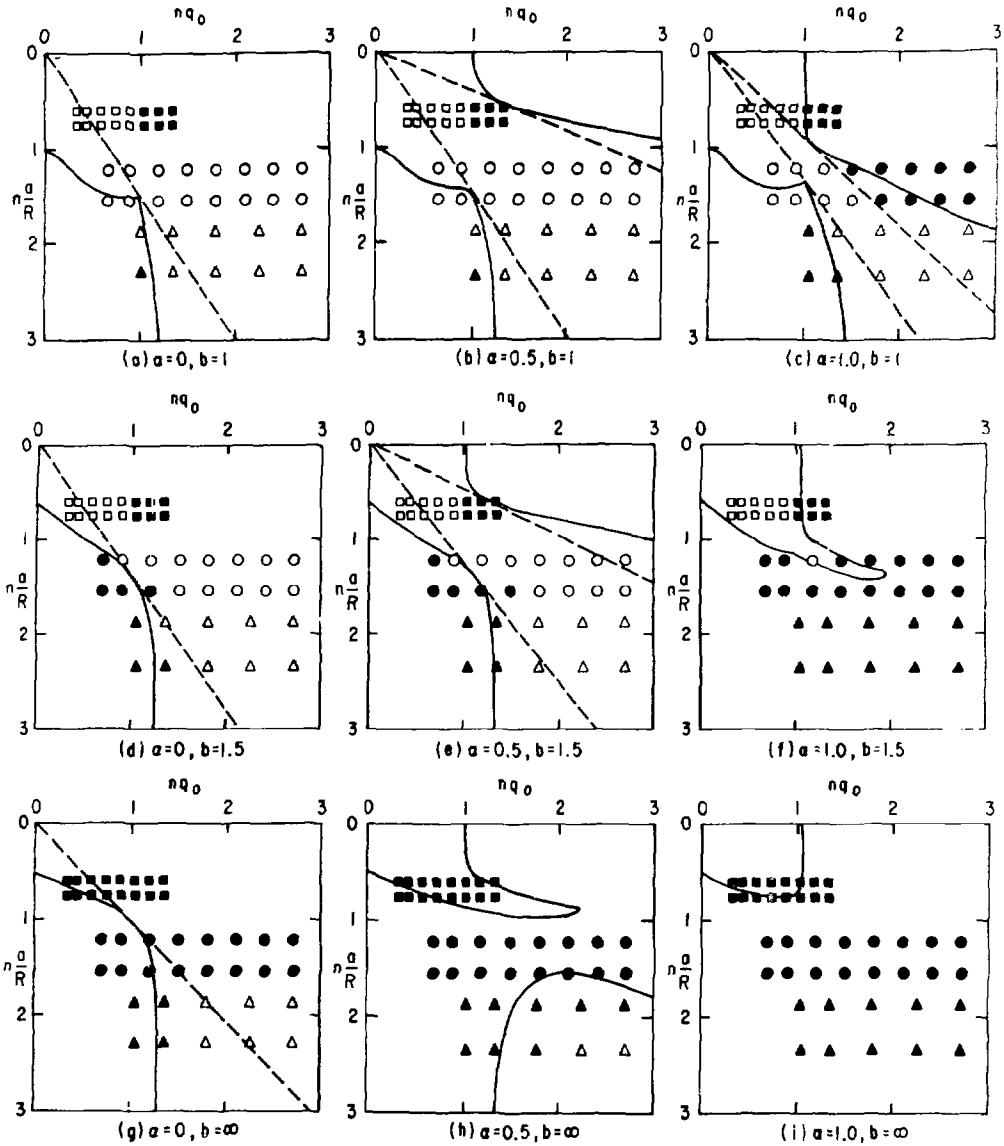

Fig. 10

81T0317

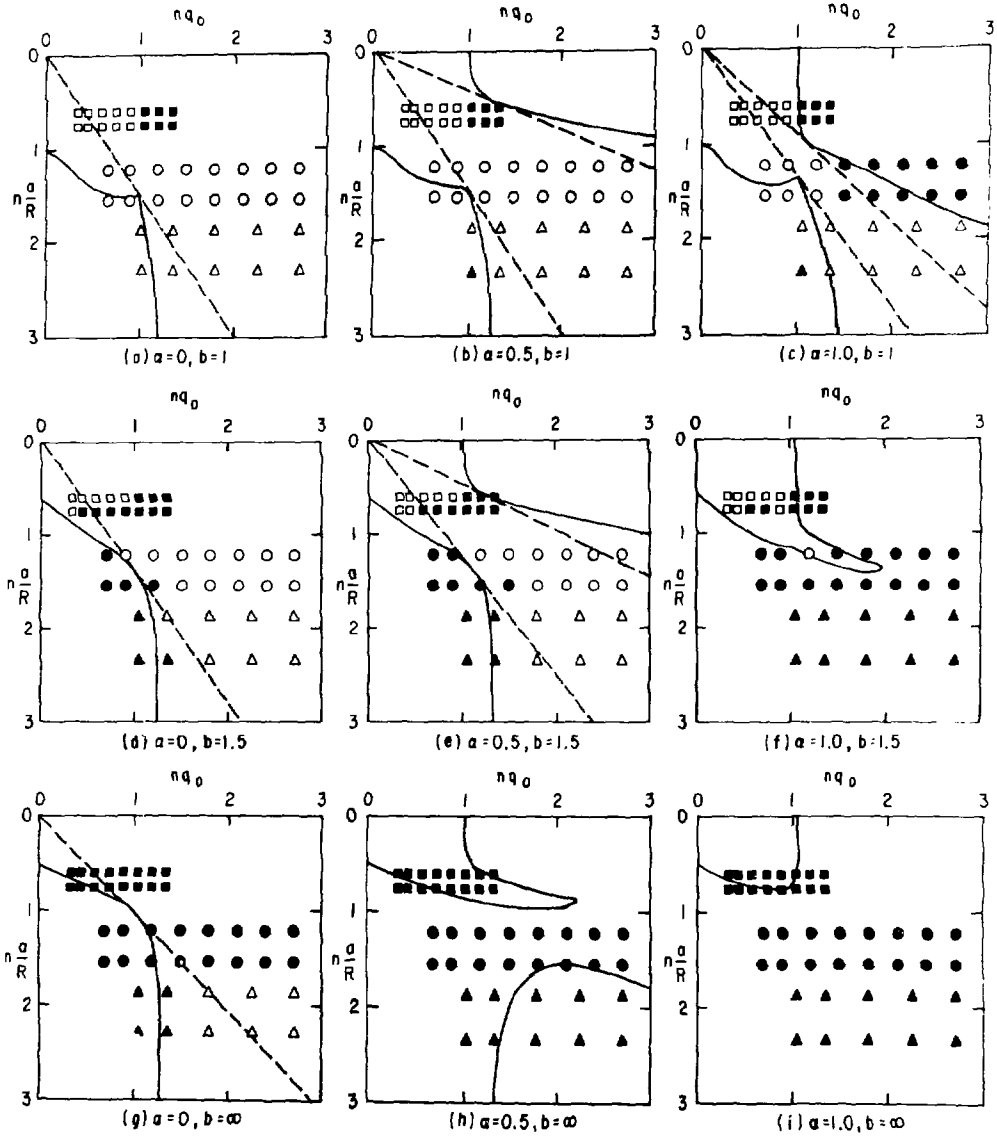

Fig. 11

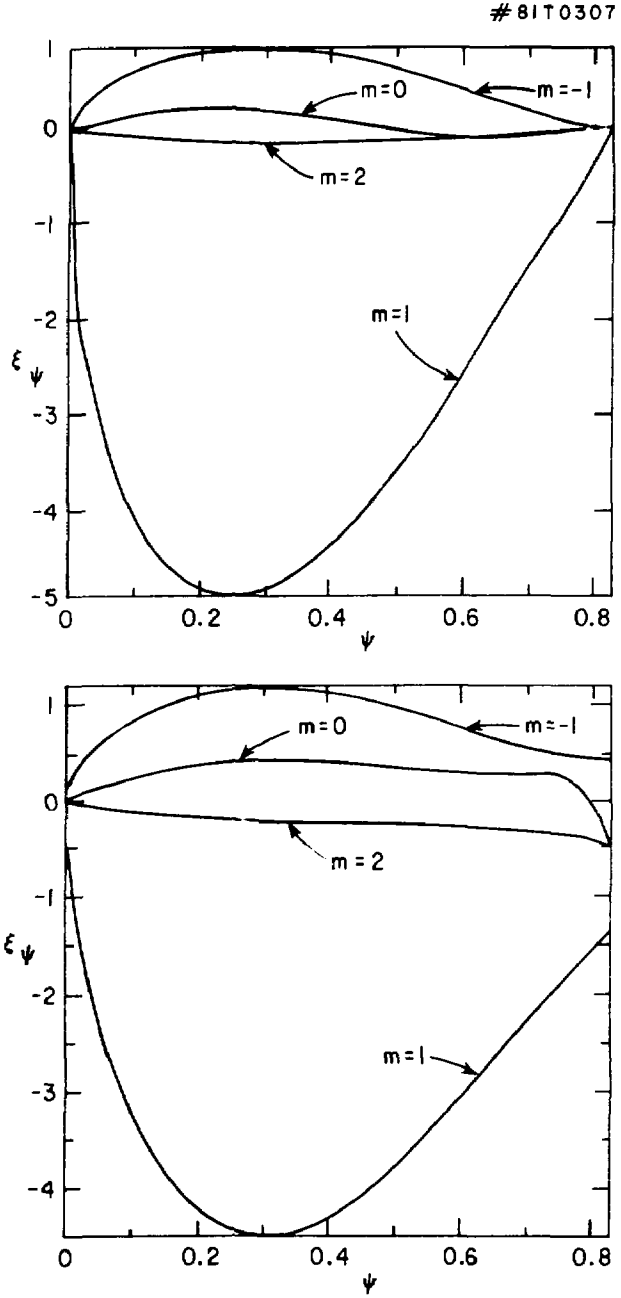

Fig. 12

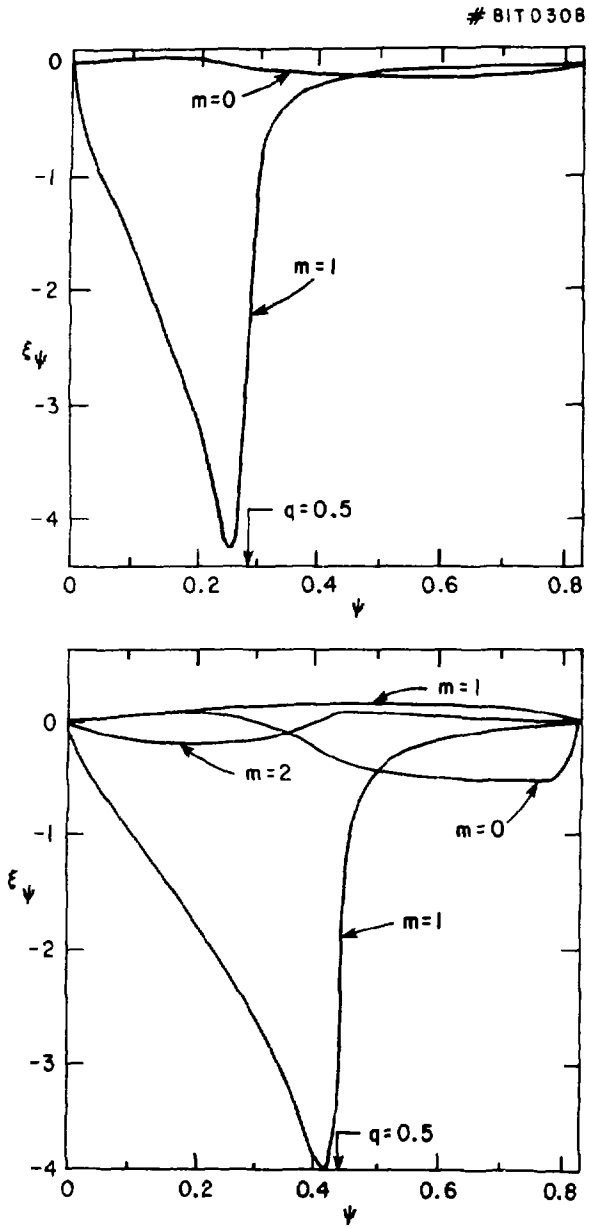

Fig. 13

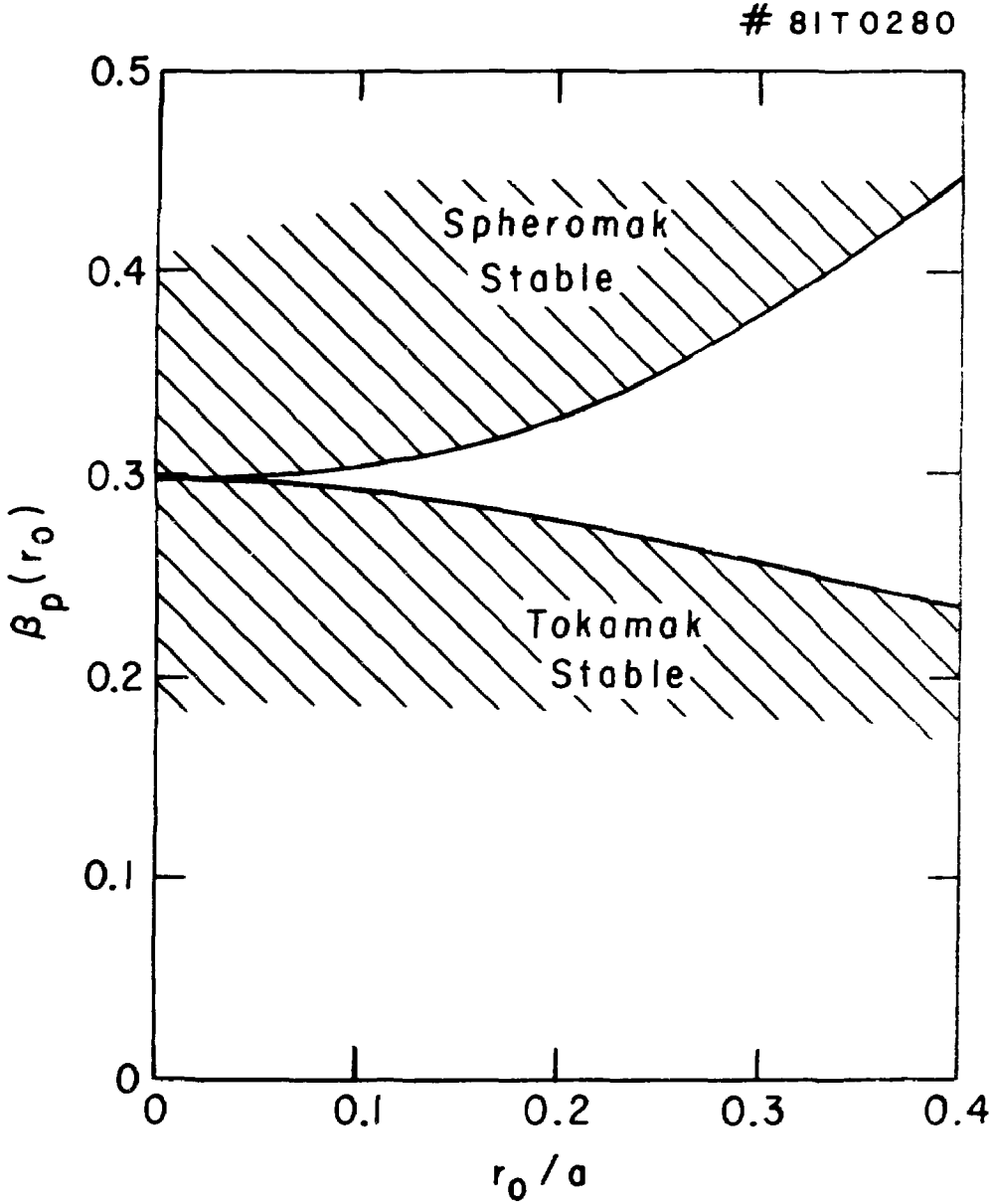
81T0280
0.5
0.4
0.3
0.2
0.1
0
Spheromak
Stable
Tokamak
Stable
$\beta_p(r_0)$
0
0.1
0.2
0.3
0.4
r_0/a

Fig. 14

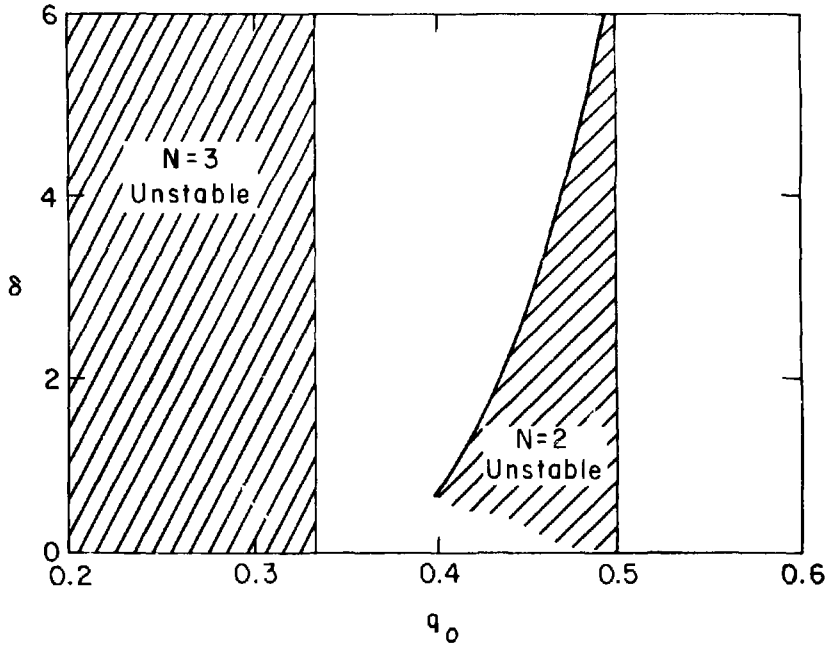

Fig. 15

#81T0046

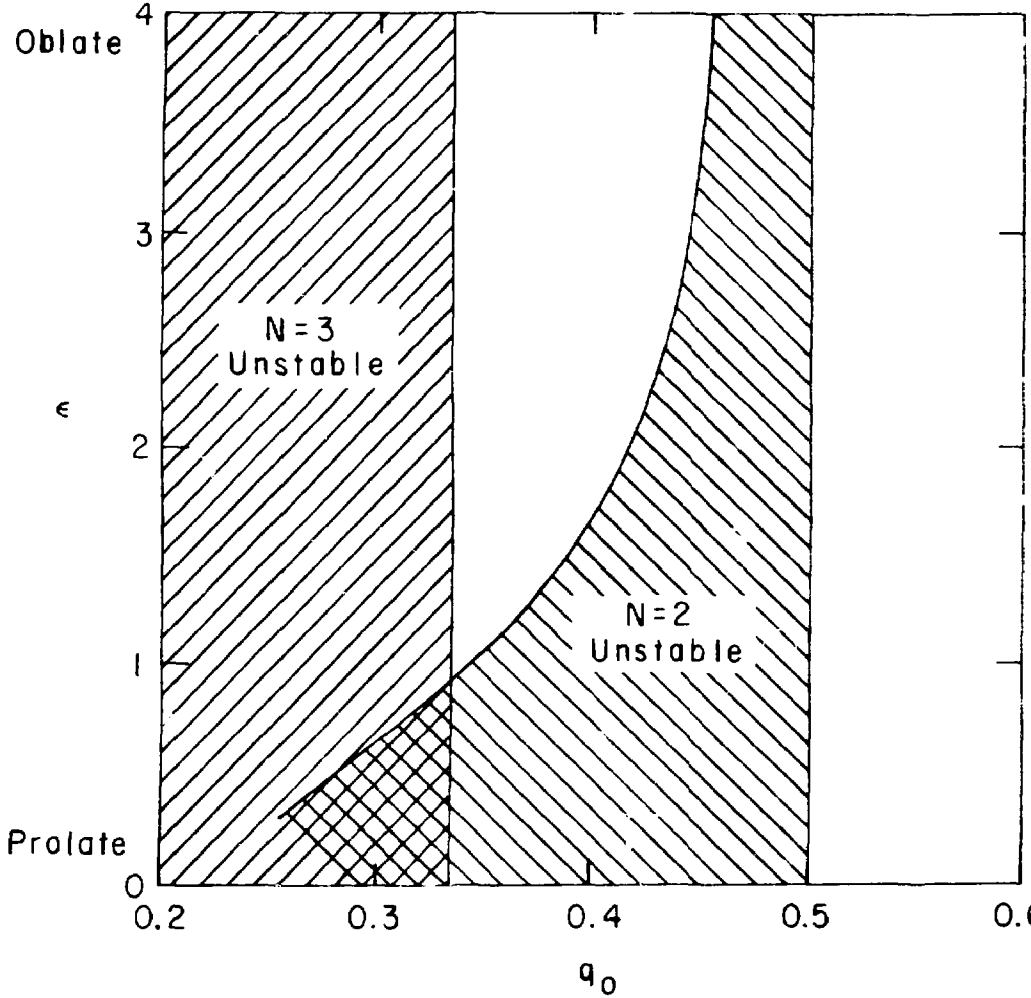

Fig. 1

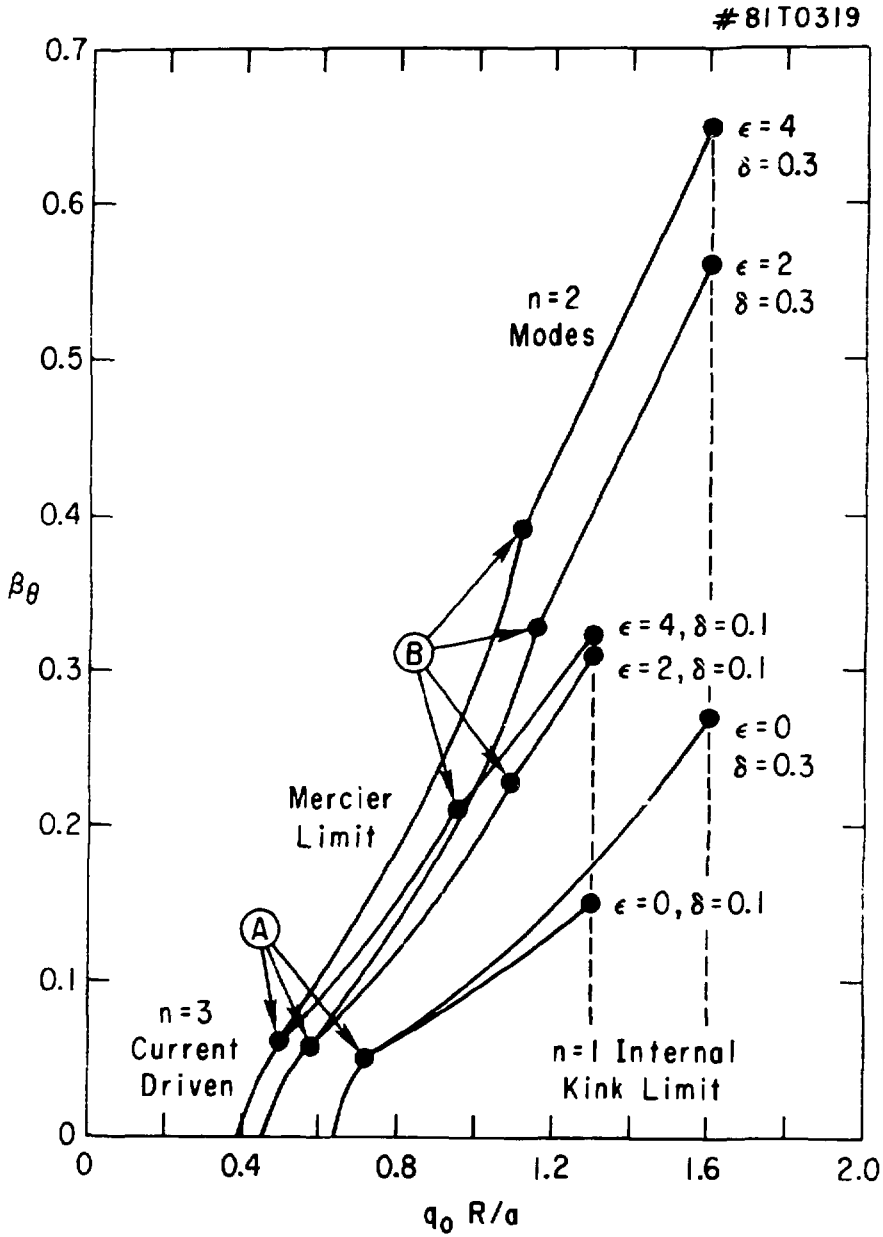
#81T0319
0.7
0.6
0.5
0.4
0.3
0.2
0.1
0
β_θ
0
0.4
0.8
1.2
1.6
2.0
q_0 R/a
$\epsilon = 4$
$\delta = 0.3$
$\epsilon = 2$
$\delta = 0.3$
n=2
Modes
B
$\epsilon = 4, \delta = 0.1$
$\epsilon = 2, \delta = 0.1$
$\epsilon = 0$
$\delta = 0.3$
Mercier
Limit
$\epsilon = 0, \delta = 0.1$
A
n=3
Current
Driven
n=1 Internal
Kink Limit

Fig. 17